HHS Public Access

Author manuscript

Nat Neurosci. Author manuscript; available in PMC 2010 August 01.

Published in final edited form as:

Nat Neurosci. 2010 February ; 13(2): 213–222. doi:10.1038/nn.2458.

Representing information in neuronal cell assemblies: Persistent activity in the dentate gyrus mediated by semilunar granule cells

Phillip Larimer and **Ben W. Strowbridge**

Department of Neurosciences, Case Western Reserve University, Cleveland, Ohio, USA

Abstract

Using rat hippocampal slices, we found that perforant path stimulation evokes long-lasting barrages of synaptic inputs in subpopulations of dentate gyrus mossy cells and hilar interneurons. Synaptic barrages could trigger persistent firing in hilar neurons. We found that synaptic barrages originate from semilunar granule cells (SGCs), glutamatergic neurons in the inner molecular layer that generate long-duration plateau potentials in response to excitatory synaptic input. MK801, nimodipine, and nickel all abolished stimulus-evoked plateau potentials in SGCs, and synaptic barrages in downstream hilar neurons, without blocking fast synaptic transmission. Hilar up-states triggered functional inhibition in granule cells that persisted for >10 s. Hilar cell assemblies, assayed by simultaneous triple and paired intracellular recordings, were linked by persistent firing in SGCs. Population responses recorded in hilar neurons accurately encoded stimulus identity. Stimulus-evoked up-states in dentate gyrus represent a potential cellular basis for hippocampal working memory.

Keywords

Hippocampus; plateau potential; working memory; brain slice; patch clamp; 2-photon Ca^{2+} imaging; paired recording; mossy cell

While most CNS neurons respond transiently to synaptic input, neurons in neocortical regions[1–3], and in the hippocampus[4,5], can fire persistently in response to brief stimuli. Persistent firing in these neurons typically lasts for multiple seconds and often is associated with working memory in delayed-response tasks[6,7,4]. In nonhuman primates, activity in spatially-tuned “delay neurons” in prefrontal neocortex can predict whether specific stimuli will be correctly recalled. The selective activation of delay neurons during working memory tasks, and the correlation between delay-period discharges and performance[6,7,4], both argue strongly that persistent activity is intimately associated with memory function. While many studies have demonstrated extracellularly-recorded delay period discharges in rodents[8] and

Correspondence: Dr. Ben W. Strowbridge, Dept. of Neurosciences, Case Western Reserve Univ., 10900 Euclid Ave., Cleveland, OH 44106, (216) 368-6974, bens@case.edu.

AUTHOR CONTRIBUTIONS

The study was designed, data analyzed, and manuscript written by P.L. and B.W.S. The experimental work was performed by P.L.

primates[6,7], the cellular mechanism responsible for this behavior has not been established. Persistent firing also has been reported in subcortical brain areas [9,10], suggesting that this activity may represent a fundamental form of brain dynamics.

The persistent firing mode recorded in single units *in vivo* presumably reflects a network up-state since most cortical principal neurons do not fire persistently in response to brief depolarizing steps *in vitro* under physiological conditions[11,12]. Cell-autonomous persistent firing modes have been reported in several brain regions, but not in cortical neurons typically associated with working memory. Since there have been no previous *in vitro* models of cortical up-states that exhibit distinct stimulus-specific persistent activity patterns[9], it has been difficult to determine if intrinsic persistent firing modes are engaged during working memory tasks. Hebb[13], and other researchers[14–16], proposed that reverberating activity circulating through excitatory synaptic networks might mediate persistent discharges in cortical regions. While possible to implement in precisely-tuned computer simulations[14,17,18], the fine control over synaptic strengths required to maintain up-states over seconds in biophysically realistic neurons lacking intrinsic persistent firing modes raises doubts as to the feasibility of this mechanism.

The dentate gyrus is an attractive brain region in which to examine the cellular basis of persistent network activity. The principal neuron in the dentate, the granule cell (GC), forms the first relay in the hippocampal trisynaptic circuit and likely functions to generate transient, sparse representations of complex polysensory input patterns from entorhinal projection neurons. Hilar neurons also exhibit performance-linked persistent firing during cross-sensory modality delayed match-to-sample tests[4], though the cellular mechanism mediating this activity is unknown.

Using acute rat hippocampal slices, we find that perforant path stimulation triggers reproducible patterns of persistent firing in subpopulations of hilar cells that encode information about stimulus identity. Persistent firing in hilar neurons results from prolonged discharges in a recently identified dentate gyrus cell type: the semilunar granule cell (SGC[19]). We find that these neurons, located in the inner molecular layer, receive potent glutamatergic input that can trigger plateau potentials maintained by voltage-gated Ca^{2+} channels. The synaptic interaction between a relatively rare population of broadly-projecting excitatory neurons that generate stable plateau potentials and downstream local circuit networks represents a novel, and potentially generalizable, mechanism that enables transient input to trigger persistent firing in synaptically-coupled networks.

RESULTS

Prolonged synaptic barrages in hilar neurons

Intracellular recordings from dentate hilar neurons typically are dominated by large-amplitude spontaneous synaptic potentials (Fig. 1), as described in previous studies[20–22]. In addition to spontaneous EPSPs, stimulation of axons of entorhinal cortical neuron (perforant pathway, PP) reliably evoked disynaptic EPSPs in both mossy cells and hilar interneurons. Evoked EPSPs could be recorded in response to minimal intensity stimulation and were abolished by antagonists of ionotropic glutamate receptors (10 μM NBQX; Fig. 1b).

Ongoing spontaneous synaptic activity in hilar neurons was unaffected by single or paired PP stimuli at threshold for evoking minimal disynaptic EPSPs (Fig. 1c; $P>0.05$; $n=12$ cells).

In many cortical brain regions, increasing stimulus intensity beyond minimal levels tends to recruit potent inhibitionthat diminishes the excitability of principal cells. In dentate hilar cells, by contrast, supraminimal PP stimulation often triggered persistent spiking resulting from long-lasting barrages of synaptic potentials (Fig. 1c). Spontaneous EPSP frequency increased by more than 5-fold during these barrages ($P<0.001$; $n=12$; Fig. 1e). Stimulation-evoked synaptic barrages occurred in both mossy cells ($n=101$, 9 visualized) and hilar interneurons ($n=32$, 3 visualized). Barrages in voltage-clamped hilar cells were composed of excitatory and inhibitory synaptic responses (Supplementary Fig. 1). Synaptic barrages recorded in mossy cells and hilar interneurons were abolished by NBQX (5 μM; $n=5$; Fig. 1d). Synaptic barrages that increased spontaneous EPSP frequency at least 2-fold were not evoked by minimal (0/22 experiments), or twice-minimal (0/6) PP stimuli but were often evoked by 3x minimal stimulation (7/10). Ten-times minimal PP stimuli reliably triggered barrages in most experiments (11/12; Fig. 1f).

Epochs of persistent synaptic input to hilar neurons could be evoked repetitively (Supplementary Fig. 2a,b), suggesting that these responses were not associated with pathological changes. We also did not observe changes in intrinsic properties of hilar neurons following synaptic barrages (Supplementary Fig. 2c–g). Synaptic barrages were not abolished by injection of 1–2 s duration hyperpolarizing steps that either coincided with the PP stimuli or occurred after the barrage was initiated ($n=3$), suggesting that barrages did not requiring persistent spiking in that neuron.

Extracellular multiunit activity (MUA) recordings (Fig. 2a,b) demonstrate that dentate up-states evoked by PP stimulation reflect synaptic activation of populations of hilar neurons, rather than intrinsic responses in individual neurons. Both hilar MUA (Fig. 2c) and cell-attached recordings from hilar cells (Fig. 2d) showed prolonged spiking discharges in hilar cells following transient PP stimulation. Hilar cell discharges recorded in both extracellular and cell-attached configurations decayed monoexponentially (Hilar MUA $\tau=7.9\pm0.5$ s; cell-attached recordings $\tau=6.9\pm0.6$ s; $n=6$ each; Fig. 2c,d,f). Persistent firing in hilar neurons required activation of ionotropic glutamate receptors and was reversibly blocked by NBQX (5 μM) and D-APV (25 μM; $n=6$; Fig. 2e). The inhibitory component of PP-evoked synaptic barrages also required activation of ionotropic glutamate receptors ($n=5$; Fig. 2g).

Mechanism of hilar network up-states

Persistent synaptic barrages recorded in hilar neurons may reflect prolonged discharges in presynaptic neurons, modulation of the local environment near hilar synapses that promote asynchronous neurotransmitter release, or a combination of these mechanisms. We attempted to identify correlated synaptic responses within up-states in simultaneously recorded pairs of hilar neurons that would be expected from spiking in common presynaptic cells. An example of near-synchronous EPSPs recorded during an up-state in a pair of mossy cells is shown in Supplementary Fig. 3a. The frequency of near-coincident EPSPs was significantly elevated in this paired recording (153% of expected frequency; significantly greater than shuffled controls, $P<10^{-6}$; based on Poisson cumulative distribution[23]) and in a

population of 13 paired hilar cell recordings analyzed (121±4.2% of control, significantly elevated; $P<0.001$; *t*-test; Supplementary Fig. 3), suggesting that network up-states reflect discharges in presynaptic neurons that form divergent excitatory connections onto hilar neurons. Increased EPSP correlation also could reflect nondivergent presynaptic neurons that become synchronized following PP stimulation by phase-locking local interneurons.

We also tested whether blockers of potential extracellular signaling molecules could occlude hilar up-states. Blockade of nitric oxide (NO) signaling with ODQ (10 μM), an inhibitor of soluble guanylyl cyclase, failed to eliminate hilar up-states in 3/4 experiments. Blockade of CB1 receptors with AM251 (10 μM) also failed to abolish hilar up-states in 10/11 experiments. Hilar up-states also could be evoked both before and after application of atropine (1–5 μM; $n=6$) and SYM2081 (0.1–1 μM, $n=4$), antagonists for muscarinic and kainate receptors, respectively. Finally, we tested whether hilar up-states were dependent on a narrow extracellular K^+ concentration range. We found that PP stimulation reliably triggered hilar up-states at both physiological K^+ concentrations (3 mM; $n>50$) and with elevated extracellular [K^+] (5 mM; $n=4$). These negative results suggest that barrages recorded in hilar cells reflect spiking activity in synaptically-coupled networks, rather than slow changes in the concentration of signaling molecules or ions.

We next searched for the source of the persistent synaptic input to hilar neurons during up-states. PP stimulation reliably triggered up-states in hilar neurons in slices in which either the CA3 region or entorhinal cortex was removed ($n=3$ each; Supplementary Fig. 4), suggesting neither brain region was the primary source of persistent synaptic drive to hilar neurons. PP stimulation triggered relatively weak synaptic barrages in CA3 pyramidal cells with significantly smaller increases in EPSP frequency (8.8±4.2 Hz; $n=7$) than recorded in hilar neurons (33.6±7.3 Hz; $n=12$; $P<0.02$). Synaptic barrages in CA3 neurons also were composed of primarily small-amplitude EPSPs, compared with barrages in both hilar interneurons and mossy cells that are typically dominated by large-amplitude EPSPs. Hilar up-states also are unlikely to result from reverberant synaptic loops among hilar cells since mossy cells, the major glutamatergic cell type in the hilus[24,25] only rarely contact other mossy cells within the same brain slice[26,27]. While granule cells also can form recurrent excitatory circuits with hilar mossy cells[25], we never observed discharges in granule cells during hilar up-states (0/35 GCs tested).

Unexpectedly, multi-unit recording electrodes consistently demonstrated PP-evoked persistent spiking when placed in the inner molecular layer (IML; $n=6$; Fig. 3a). Cell-attached recordings of IML neurons also fired persistently following PP stimulation (9/9 IML neurons tested; Fig. 3b). Cell-attached recordings from neurons in the granule cell layer (GCL) did not show persistent firing when tested under the same conditions (0/4 GCs; Fig. 3b). Since much of the synaptic drive to hilar cells during up-states is excitatory (Supplementary Fig. 1), spiking in glutamatergic semilunar granule cells (SGCs[19]) represents a likely source of persistent activity. We tested the hypothesis that SGCs become persistently active following PP stimulation by recording from 58 SGCs in the IML and from 25 GCs in the GCL. More than 72% of the SGCs tested generated prolonged depolarizations following PP stimulation (42/58 SGCs with response integral>2 mV*s; Fig. 3c), a response observed less frequently in GCs (2/25 cells) when tested with similar

stimulus intensities (P>0.05) and at similar membrane potentials (−72.7±0.9 mV in SGCs vs. −69.8±1.3 mV in GCs; P>0.05). On average, the response integrals in these experiments were significantly larger in SGCs (23.8±4.5 mV*s; n=58) than in GCs (−5.75±2.2 mV*s; n=25; $P<10^{-4}$; Fig. 3d; stimulus intensities not significantly different between cell-attached and whole-cell SGC recordings; P>0.05). Since these responses were recorded near the reversal potential of $GABA_A$ receptor-mediated IPSPs (−74.0±1.7 mV; n=10), we also examined SGCs and GCs responses in a subset of neurons at the same, more depolarized, membrane potential (SGCs: −60.3±0.9 mV; GCs: −60.3±1.5 mV). SGCs recorded at −60 mV also generated plateau responses (mean integral=12.2±5.0 mV*s; n=36 cells), significantly greater integrals than GC responses at the same potential (−9.4±2.4 mV*s; n=21; P<0.01). We also confirmed that filled SGCs identified by both morphological and physiological characteristics[19] generated plateau potentials (24.5±13.0 mV*s plateau integral; n=3). The voltage integrals measured in these whole-cell intracellular recordings are likely to underestimate the actual plateau depolarization evoked by PP stimulation since sequential cell-attached and whole-cell intracellular recordings from SGCs consistently exhibited less persistent spiking (n=4). Injecting hyperpolarizing steps (1–4 s duration, >30 mV hyperpolarization) did not truncate plateau potentials in 8 SGCs tested.

The majority of GCs tested (68%), and a minority of SGCs (22%), appeared to be inhibited during hilar cell up-states. The absence of PP stimulus-evoked up-states in GCs did not reflect dendritic truncation since visualized GCs that had intact dendritic arbors generated prolonged hyperpolarizations following PP stimulation (Supplementary Fig. 5). We also observed a short-latency EPSP immediately following PP stimulation (Fig. 3c, *inset*) in most GCs, reflecting preserved monosynaptic excitatory input to GCs. Finally, we used brief depolarizing test pulses to verify that GCs were functionally inhibited during dentate gyrus up-states. The latency to step-evoked APs was significantly delayed for >10 s after PP stimulation (n=6; P<0.05 to 0.005; Fig. 3e,f). Most of the granule cells that were not inhibited following PP stimulation showed no measurable response (6/25); 2 GCs generated weak depolarizations (<2 mV sustained depolarization).

In paired recordings, the PP stimulus threshold for triggering plateau potentials in SGCs was similar to the threshold for evoking synaptic up-states in hilar cells (Fig. 4a). Graded amplitude plateau potentials occurred in SGCs between individual stimuli during trains of PP shocks that elicited hilar up-states. Changes in the frequency of SGC discharges following PP stimulation closely paralleled the increase in EPSC frequency in hilar neurons recorded in separate experiments (R^2=0.86; n=6 SGCs and 13 hilar cells; Fig. 4b,c). The ratio of hilar EPSC frequency to SGC firing frequency was 3.9±0.2 during the 4 s after PP stimulation. Given the mean failure rate of SGC-to-hilar cell synapses (0.46; ref[19]), PP stimulation likely triggers plateau potentials in at least 7 SGCs. Consistent with this model, we failed to trigger up-states in hilar cells following prolonged intracellular depolarization of individual SGCs (0/6 dual intracellular recordings; 0/25 simultaneous SGC intracellular/hilar MUA recordings).

Plateau potentials in SGCs are triggered by NMDA receptors

We next asked why SGCs generate long-duration plateau potentials in response to PP stimulation protocols that inhibit GCs. One possibility is that SGCs receive different types, or densities, of synaptic input than GCs. We explored this possibility by recording pure PP-evoked EPSCs in SGCs and GCs in the presence of gabazine (20 μM) and CGP55845 (10 μM) to block fast and slow inhibitory GABAergic responses. As previously reported[19], the amplitude of minimal excitatory responses was not significantly different between SGCs and GCs (P>0.05; Fig 5). We also observed no difference in the stimulus intensities required to evoke minimal EPSCs in SGCs (10.3±0.5 μA) and GCs (12.3±1.1 μA; P>0.05). Increasing the stimulus intensity above levels required to evoke minimal, all-or-none EPSCs, however, had markedly different effects on SGCs and GCs. Doubling the stimulus intensity from minimal levels only increased NMDA receptor-mediated EPSCs in GCs by 4.5±1.1-fold, while SGC EPSC amplitude increased by 42.6±9.7-fold. At twice minimal stimulus intensity, SGCs had significantly larger amplitude EPSCs recorded both at +55 mV (P<0.0005; Fig. 5c) and at −80 mV (P<0.001; Fig. 5b). The same pattern, with the amplitude of EPSCs recorded in SGCs increasing more rapidly with stimulus intensity than EPSCs recorded in GCs, continued at 3x minimal intensity (n=4 and 6 for SGCs and GCs, respectively). The parallel changes in EPSC amplitude recorded at both −80 and +55 mV argue that SGCs receive substantially larger glutamatergic drive than GCs in response to supraminimal PP stimuli.

Several lines of evidence suggest that plateaus in SGCs were triggered by ionotropic glutamate receptors. Reducing Na^+ currents with partial NMG substitution blocked action potentials in SGCs but did not significantly diminish plateau potentials triggered by pressure application of glutamate (plateau voltage integral=69±8% of control; P>0.05; n=3). Plateau potentials evoked by pressure application of glutamate are likely initiated by inward Ca^{2+} currents through NMDA receptors[28]. Plateau potentials with comparable voltage integrals (39.2 mV*s; n=2) could be evoked in SGCs loaded with Ca^{2+} chelators (10 mM BAPTA), a treatment that decreased spike AHP amplitude by more than 50%. Synaptic stimulation also triggered plateau potentials in SGCs loaded with GTP/GDP analogs that occlude G-protein signaling (GTPγS, 500 μM, n=8; GDPβS, 1 mM, n=2). Plateau potentials also were insensitive to 5 μM PPADs (n=4) and 2 μM NF279 (n=2), antagonists of P2X receptors that block ATP signaling. SGC plateau potentials, but not hilar up-states, could be evoked by PP stimulation in slices with cuts between the granule cell layer and hilus, lesions that undercut the recorded SGC (SGC voltage integral=117.1±20.2 mV*s; ΔEPSP frequency=0.38±1.1 Hz in simultaneously recorded hilar cells; n=3 paired recordings in cut slices; Supplementary Fig. 6), suggesting that plateau potentials were not maintained by persistent input from mossy cells.

We asked whether glutamatergic EPSPs are required to trigger plateau potentials in SGCs. The combination of NBQX (5 μM) and MK801 (10 μM) abolished evoked plateaus in 4/4 SGCs tested. Blockade of NMDA receptors alone with MK801 (10 μM) also strongly attenuated evoked SGC plateaus (response integral decreased from 57.5±15.9 to 6.8±2.7 mV*s; significantly different; P<0.02; n=4; Fig. 6a,c). Also consistent with this model, we found that plateaus could be triggered in SGCs by brief focal application of NMDA (0.2–1

mM) in the IML (NMDA response integral=81.2±14.8 mV*s; *n*=6; Supplementary Fig. 6b). NMDA-evoked plateau potentials triggered spike discharges in SGCs that resembled responses evoked by synaptic stimulation.

Blocking plateaus in SGCs eliminates synaptic up-states

We next tested whether persistent firing triggered by plateau potentials in SGCs might generate the synaptic barrages recorded in hilar neurons. We first blocked the initiation of plateau potentials in SGCs using the noncompetitive NMDAR receptor antagonist MK801. In 7/7 hilar cell recordings, MK801 abolished evoked hilar up-states (96% decrease in ΔEPSP frequency; $P<0.0005$; Fig. 6b,d) without affecting the initial EPSP response in hilar neurons (EPSP slope=108.0±13% of control; $P>0.05$; $n=6$; Fig. 6b *inset*, Fig. 6e). In SGCs, blockade of NMDA receptors also did not affect the EPSC evoked by 2x minimal stimulation (97.1±15.2% of control following 50 μM D-APV; not significantly different from 100%; $P>0.05$; $n=6$). Short-latency evoked EPSPs, and the normal on-going spontaneous EPSPs in hilar cells, were blocked by the subsequent addition of NBQX (10 μM; $n=3$; Fig. 6e). The ability of MK801 to selectively block both plateau potentials in SGCs and synaptic up-states in hilar neurons is consistent with hilar up-states originating from subpopulations of persistently-firing SGCs.

We also used blockers of voltage-gated Ca^{2+} channels (VGCCs) to reduce the excitability of SGCs to test the relationship between persistent firing in SGCs and hilar up-states. Simply switching to a low Ca^{2+} ACSF solution abolished synaptically triggered plateau potentials in SGCs ($n=5$; Supplementary Fig. 7), but also reduced evoked responses. Nimodipine, a dihydropiridine antagonist of L-type VGCCs[29], greatly attenuated synaptic barrages in hilar neurons (77% decrease in ΔEPSP frequency; $P<0.005$; $n=6$; Fig. 7a–c; 10 μM) without affecting the short-latency EPSP evoked by single PP stimuli (*inset* in Fig. 7b). Nimodipine also blocked most of the long-duration plateau potential recorded in SGCs following PPstimulation (93% reduction in voltage integral; $P<0.005$; $n=4$; Fig. 7d–f). We typically recorded brief plateau responses following individual PP stimuli in nimodipine (Fig. 7e; example in 20 μM nimodipine). These residual, short-duration plateau responses were blocked by the subsequent addition of 200 μM nickel (Fig. 7d–f; $n=4$), an antagonist of low-threshold (T-type) VGCCs[30],[31].

Direct somatic depolarization of individual SGCs failed to trigger long-duration plateaus but reliably triggered brief plateaus in which membrane potentials stabilized near firing threshold for >10 ms (Supplementary Fig. 7a; $n=10$). In 8/10 cells, these active plateau potentials triggered action potentials after the offset of the depolarizing current step. Intrinsic plateau potentials were reversibly blocked by 200 μM nickel (Supplementary Fig. 7b) and triggered Ca^{2+} influxes detected using nonraster 2-photon imaging ($n=4$; Supplementary Fig. 7c,d). Together, these results are consistent with the hypothesis that SGCs express both low- (T-type) and high-threshold VGCCs.

Next, we used nickel to test whether activation of T-type VGCCs are required to evoke plateau potentials in SGCs. Nickel abolished plateau potentials in SGCs (200 μM; $P<0.005$; $n=6$; Fig. 7g,i). The same concentration of nickel that selectively abolished plateau potentials in SGCs also blocked PP-evoked hilar up-states (90% reduction in ΔEPSP Freq;

PP-evoked enhancement in EPSP frequency eliminated in 4/4 hilar cells tested; $P<0.002$; Fig. 7h,j). Nickel blocked network up-states without impairing fast glutamatergic transmission onto hilar neurons (EPSP slope=80.3±15 % of control; $n=4$; mean EPSP slopes not statistically different; $P>0.05$; Fig. 7h, *inset*; Fig. 7k). The ability of nimidipine and nickel to selectively, and independently, abolish both plateau potentials in SGCs and synaptic barrages in hilar neurons is consistent with the hypothesis that hilar up-states originate from persistent firing in a subpopulation of SGCs.

Stimulus-specific hilar cell assemblies

Finally, we employed multiple recordings to test whether stimulation of different entorhinal inputs generates up-states in distinct subpopulations of hilar cells. We observed heterogeneity in both the kinetics and magnitude of the PP-evoked up-states in simultaneous triple recordings. In the example in Fig. 8a, synaptic barrages were evoked only in 2/3 mossy cells by PP stimulation at site *A* while stimulation at another site (*B*) triggered up-states in all three mossy cells. Stimulus-specific response patterns were repeatable across multiple trials. This heterogeneity was limited to the prolonged synaptic barrage component of the response; stimuli at both positions evoked short-latency EPSPs in all three mossy cells. Up-state heterogeneity did not appear to reflect topology in the network responses since the cell bodies of all three mossy cells were near each other (Supplementary Fig. 8), nor did it necessarily reflect proximity to the activated stimulating electrode since MC2 responded most vigorously to the more distant stimulus *B* and only weakly to the closer stimulus *A*. The heterogeneity in responses in closely-spaced hilar cells with expansive, multipolar dendrites implies a high degree of synapse-specificity in SGC-to-hilar cell connections.

We analyzed the structure of the network up-states evoked by different PP stimuli by creating trajectory plots that reflected the instantaneous EPSP frequency in each hilar cell recording (see Supplementary Fig. 9 for details). The trajectories evoked by stimuli *A* and *B* in the triple recording in Fig. 8a were nonoverlapping in both 2 (using only MC1 and MC3, Fig. 8b) and 3 dimensional (not shown) plots. We represented the structure of the hilar network up-states evoked by stimuli *A* and *B* in Fig. 8c using population activity vectors[32,33] calculated from the mean ΔEPSP frequencies during responses. Mean activity vectors (thick lines) were calculated from responses to 10 alternating *A*/*B* stimuli (thin lines). Population vector representations of the network responses to stimuli *A* and *B* were statistically different using either Euclidean distance or angle metrics (both distance and angle $P<10^{-6}$; $n=10$ trials). Supplementary Fig. 10 illustrates another example of stimulus-specific population vectors calculated from a different triple recording.

Responses in hilar cell assemblies were closely linked to stimulus identity. We tested whether responses to different stimuli were distinguishable by plotting absolute differences in population vector angle (Y axis in Fig. 8d) and Euclidean distance (X axis) between all combinations of responses to stimulus *A* and *B* (“*trans”;* red symbols in Fig. 8d). Differences between responses to stimuli A and B were statistically distinguishable from random combinations of trials of the same stimulus type (*A* vs. *A* and *B* vs. *B*, both “*cis*”; $P<10^{-4}$; Hotelling T^2-test; Fig. 8d). Alternating between stimulus *A* and *B* evoked large

changes in both vector angle and distance response metrics. These changes in population responses were significantly greater than those evoked by comparing responses to repeated trials of the same stimulus ($P<10^{-6}$).

We also tested the association between hilar cell assembly responses and stimulus identity by calculating the distance from optimal separation planes. Distances from these planes were reproducible over multiple responses to stimuli *A* and *B* (Fig. 8e). The mean distances of the cell assembly responses evoked by stimulus *A* and *B* were statistically different and were separable to at least $P<0.05$ in 6/7 experiments (Fig. 8f). Separation planes generated by linear discriminant analysis correctly categorized 96% of responses to stimulus *A* and *B* (47/49 trials; $n=7$ experiments). No statistically significant differences in a parallel analysis where stimulus identity was randomized (black symbols in Fig. 8f; $P>0.05$; $n=7$ experiments).

Simultaneously-recorded hilar cell responses correctly predicted stimulus identity (80±8% accuracy averaged over 6 s; Fig. 8g, black symbols; $n=7$ experiments). The predictions of stimulus identity based on sampled network up-states were significantly better than expected by chance, and by predictions based on spontaneous activity before the stimulus (both $P>0.05$). Short (1s) windows of hilar cell activity predicted stimulus identity for ~6 s, 2 s beyond the data used to generate separation planes. Integrating successive predictions from these snapshots only slightly increased accuracy (to 90±7%; Fig. 8g, red symbols) but enabled stimulus identity to be predicted over a longer (>10 s) time window after PP stimulation (red asterisks). These results demonstrate that barrages of synaptic input in hilar neurons during up-states can encode stimulus identity.

DISCUSSION

We find that transient perforant path stimulation triggers long-lasting synaptic barrages in hilar cells that arise from persistent firing in SGCs. The up-states we recorded in mossy cells and hilar interneurons *in vitro* following PP stimulation closely resemble persistent hilar cell discharges evoked during cross-sensory modality working memory tasks *in vivo*[4]. We find that a small population of excitatory neurons in the dentate gyrus (SGCs) fire persistently following transient input, activating cell assemblies in downstream hilar neurons that encode stimulus information. The ability of dentate gyrus networks to transform transient entorhinal input into reproducible, and long-lasting hilar activity patterns may be functionally analogous to delay-period activity recorded in prefrontal cortical neurons during working memory tasks[6]. Recently, another group reported reproducible activation of a defined subset of neocortical neurons by thalamic stimulation[34]. The present report extends this concept to the dentate gyrus and represents the first example of multiple, stimulus-specific cell assemblies that can be recorded *in vitro* in a mammalian cortical region.

Hilar up-states are mediated by persistent firing in SGCs

Four lines of evidence suggest that the excitatory component of the synaptic barrages originates from persistent firing in SGCs. First, while hilar cells receive five types of excitatory synaptic input (from granule cells[35], SGCs[19], entorhinal neurons[36], CA3 pyramidal cells[37],[38] and other mossy cells[27]), barrages appear to only require SGCs.

Synaptic barrages can be evoked in slices with CA3 and entorhinal cortex removed, and nearly all GCs recorded were either inhibited or did not respond during hilar up-states. Mossy cells only rarely contact other mossy cells within the same slice (0.5% connection frequency[27]), making it improbable that hilar up-states reflect reverberant activity among networks of mossy cells. Excitatory input from mossy cells also was not required for PP input to trigger plateau potentials in SGCs, suggesting that up-states in SGCs were not maintained by persistent synaptic input from mossy cells.

Second, persistent firing in SGCs was tightly correlated with the time course of synaptic barrages recorded in hilar neurons. Persistent firing in SGCs typically occurred at 5–15 Hz, significantly slower than the frequency of spontaneous EPSPs recorded in hilar cells following PP stimulation. This finding, and the failure to initiate hilar upstates by directly depolarizing single SGCs, argues that hilar up-states reflect persistent firing in population of SGCs.

Third, both T- and L-type VGCC and NMDA receptor antagonists abolished plateau potentials in SGCs and synaptic barrages in hilar cells without blocking fast synaptic transmission. The ability of focal NMDA application in the molecular layer to trigger plateau potentials in SGCs, and the observation that PP stimulation can trigger persistent firing in SGCs in slices with cuts between the granule cell layer and hilus (Supplementary Fig. 6), both argue that network up-states originate from discharges in SGCs, rather than mossy cells.

Finally, we found no evidence supporting nonsynaptic mechanisms mediating hilar up-states. Previous studies have identified network activity modes triggered by paracrine, ephaptic, and field interactions[39]. A common feature of these nonsynaptic up-state mechanisms is a lack of target cell specificity. Up-states in the dentate gyrus, by contrast, show exquisite neuronal selectivity and involve spatially distributed subsets of hilar cells while avoiding nearby granule cells. Both the frequent synchronous EPSPs recorded in pairs of hilar cells during up-states, and the heterogeneity of hilar cell responses revealed in simultaneous intracellular recordings from nearby hilar cells, suggest that hilar up-states are driven by spiking in presynaptic glutamatergic neurons that project to subsets of hilar neurons[19], rather than the action of a diffuse extracellular signal.

Plateau potentials in SGCs can be evoked under physiological conditions, consistent with activation of regenerative, or “window” Ca^{2+} currents[40]. The relatively long duration, and sensitivity of plateau potentials in SGCs to nickel and nimodipine, makes it unlikely that SGC responses reflect NMDA receptor “spikes”[1,41]. Instead, in SGCs the interplay between Ca^{2+} currents and an outward leak current likely generates bistability, as shown in thalamocortical neurons which can achieve separations of 30 mV between the stable membrane potentials[40,42]. Our finding that nimodipine- and nickel-sensitive VGCCs are required for synaptically-evoked plateau potentials in SGCs is consistent with this mechanism. Plateau responses in SGCs typically were unaffected by hyperpolarizing current steps (20 trails in 7 SGCs, data not shown), suggesting that the relevant Ca^{2+} channels might be located in distal dendrites. Hyperpolarizing steps applied coincidentally with the PP

stimulation, or during the response, also did not affect synaptic barrages in hilar neurons (*n*=3).

We find evidence for two types of VGCCs in SGCs that contribute to the plateau response. Most of the plateau responses, especially the long latency components, was blocked by the dihydropyridine nimodipine, suggesting a critical role for L-type Ca^{2+} channels[29]. L-type VGCCs have been proposed to underlie plateau responses in other neurons[43] and can exist in a variant that activates at relatively hyperpolarized voltages that can mediate large window currents[29],[44]. We also found that nickel abolished plateau responses in SGCs without blocking fast synaptic transmission, suggesting that SGCs also express T-type VGCCs. This result is consistent with *in situ* hybridization analysis that demonstrated high expression of transcripts for nickel-sensitive $Ca_V3.2$ VGCCs in the molecular layer of the dentate gyrus[45], where SGC cell bodies are located.

Functional significance of up-states in the dentate gyrus

Persistent activity in assemblies of hilar neurons may function to generate short-term representations of stimulus features, such as stimulus novelty. Hilar neurons are uniquely situated in the hippocampal formation to receive both feedforward entorhinal input (via intermediate sparse representations generated by granule cells) and feedback input from autoassociative networks of CA3 pyramidal cells[46]. No other hippocampal neuronal population (besides CA3 neurons themselves) integrates information from both of these primary feedforward and feedback excitatory pathways. Through this synaptic pathway integration, hilar cells may detect stimulus novelty by comparing the spatio-temporal structure of entorhinal input patterns with the output of local CA3 networks during prompted recall.

Previous *in vivo* recording studies have demonstrated persistent firing in hilar neurons during working memory tasks[4], similar to firing modes during up-states that we find *in vitro*. Hilar cells appear to be involved in processing long-term memory during consolidation since hilar cell loss is strongly correlated with memory impairments in both human epileptic patients undergoing temporal lobe resection[47] and in animal models of traumatic brain injury[48].

We also find hilar up-states are tightly correlated with long-lasting inhibition of GCs. This profound inhibition of large populations of GCs following transient input may function to limit excitatory transmission through the hippocampal trisynaptic circuit. The prolonged up-state-associated functional inhibition we report in GCs may contribute to the “dentate gate” that prevents GCs from following repetitive entorhinal inputs[49]. Breakdown in the dentate gate has been suggested to underlie many of the pathophysiological changes during epileptogenesis[49], raising the possibility that SGCs may also play a pivotal role in regulating hippocampal excitability. We did not explore the cellular basis of this GC inhibition in this study, though many hilar interneurons synapse on GCs[50] and may generate a component of this inhibition. The identification of SGCs as the originators of up-states in the dentate gyrus provides a potential new therapeutic target for antiepileptogenic drug development.

METHODS

Methods and any associated references are available in the online version of the paper at http://www.nature.com/natureneuroscience/.

Online Methods

Animals

Horizontal slices (300 μm thick) of the ventral hippocampus were prepared from P14–25 Sprague-Dawley rats anesthetized with ketamine, as described previously[19,27]. Slices were incubated at 30°C for 30 minutes, and then maintained at room temperature until use. All experiments were carried out in accordance with the guidelines approved by the Case Western Reserve University Animal Care and Use Committee.

Electrophysiology

All recordings were performed in a submerged recording chamber maintained at 30°C and perfused with an extracellular solution containing (in mM): 124 NaCl, 3 KCl, 1.23 NaH2PO4, 1.2 MgSO4, 26 NaHCO3, 10 dextrose, 2.5 $CaCl_2$, equilibrated with 95% O_2/5% CO_2 (pH 7.3). Calcium currents were reduced in some experiments by switching to an extracellular solution with 0.2 mM Ca^{2+} and 6 mM Mg^{2+}. Extracellular multiunit recordings were made using an ER8 and ER98 amplifiers (Cygnus Technology) and tungsten monopolar electrodes (FHC). Whole-cell patch clamp recordings were made using AxoPatch 1D amplifiers (Molecular Devices) and borosilicate glass pipettes (3–10 M). In current-clamp recordings, recording electrodes contained (in mM): 140 K methylsulfate, 4 NaCl, 10 HEPES, 0.2 EGTA, 4 MgATP, 0.3 Na3GTP, 10 phosphocreatine. The internal solution used in voltage-clamp experiments contained (in mM): 140 Cs methanesulfonate, 4 NaCl, 10 HEPES, 1 EGTA, 25 TEA-OH, 5 QX-314, 4 MgATP, 0.3 Na3GTP, 10 phosphocreatine. In some experiments, 10 mM BAPTA, 0.5 mM GTPγS, or 1 mM GDPβS was added to the pipette solution. All internal solutions were adjusted to pH 7.3 and ~ 290 mOsm. Individual neurons were visualized under IR-DIC video microscopy (Zeiss Axioskop FS1) prior to patch-clamp recording.

Intracellular recordings were low-pass filtered at 2 kHz (FLA-01, Cygnus Technology) and acquired at 5 kHz (ITC-18, Instrutech) using custom software written in Matlab (Mathworks). Extracellular multiunit recordings were band-pass filtered between 100 Hz – 10 kHz and acquired at 20 kHz. Intracellular records presented were not corrected for the liquid junction potential. Cell-attached recordings were made at a tip potential of 0 mV. All drugs were obtained from Tocris Bioscience except nickel chloride, GTPγS and GDPβS which were obtained from Sigma, and Alexa594 and Oregon Green BAPTA 1 which were obtained from Invitrogen. NMDA was dissolved in HEPES-buffered saline and was pressure-injected using a Picospritzer III (Parker Hannifin). Nimodipine was dissolved in methanol at 10 mM and added to the bathing solution at 10–20 μM. Sharpened tungsten monopolar electrodes (FHC) were used for extracellular stimulation. Stimulus intensity was controlled by a constant-current stimulus isolation unit (A360, WPI).

2-Photon imaging

Fluorescent imaging was performed as described[19,27] using a BX51WI (Olympus) upright microscope and a home-built 2-photon laser scanning system based on the Verdi V10 pump laser, Mira 900 Ti:sapphire laser (both from Coherent) and a high-speed XY galvanometer mirror system (6210, Cambridge Technology). Neuronal reconstructions are presented as montages of maximal Z-plane projections.

Calcium Imaging

Intracellularly-loaded fluorescent dyes were excited at 810 nm through a 60× water-immersion objective (Olympus). Emitted light was detected through a light path that included a 700DCLPXR dichroic mirror, a BG39 emission filter (both from Chroma Technology), and a cooled PMT detector module (H7422P-40; Hamamastu). Photomultiplier output was converted into an analog voltage by a high-bandwidth current preamplifier (SR-570; Stanford Research Systems) and digitized with a NI 6111 (National Instruments). Beam steering waveforms (bidirectional, typically at 3200 lines/s) were generated using Matlab. The position of the illuminated spot was verified via position feedback signals generated by the galvanometer controller system. Laser beam intensity was controlled electronically through a Pockels cell attenuator (ConOptics) and a shutter (Uniblitz). Proximal dendrites were scanned rapidly with elliptical patterns using nonraster scan commands in 2-photon Ca^{2+} photometry experiments (200 μs temporal resolution). We replaced EGTA with 100 μM Oregon Green BAPTA1 in the internal solution in these experiments. Calcium imaging results are reported as ΔF/F.

Data analysis and statistics

Semilunar granule cells were differentiated from inner molecular layer interneurons by their responses to 2–4 s duration depolarizing current pulses. SGCs show moderate spike-frequency adaption[19], while IML interneurons fire intermittent tonic clusters of action potentials[50]. Granule cells typically adapt completely within 2–3 spikes (< 200 ms[12,19]). Hilar interneurons were differentiated from mossy cells using mean spike time and spike AHP metrics, as described previously[27]. As indicated in the text, we repeated several experiments in this study using morphologically-identified neurons (neurons filled with 100 μMAlexa594 and visualized using live 2-photon imaging). Most analyzes of synaptic up-states and plateau potentials were based on voltage or current recordings over 4 s, starting 500 ms after the last PP stimulation. We used a mean integral threshold of 2 mV*s, calculated over this 4 s window, to determine if individual SGCs or GCs responded to PP stimulation with a plateau potential. Spontaneous synaptic currents and potentials were detected automatically as described previously[27].

Input resistance was determined from the steady-state responses to small (~50 pA, 2 s duration) hyperpolarizing steps (as in Supplementary Fig. 2c). Action potential threshold was determined as the voltage when the second-derivative of the voltage trace was greater than 10% of the maximal achieved for that action potential. Action potential width was measured at threshold; action potential height was measured as peak minus threshold. Slope of hilar disynaptic responses were determined by a linear least-squares fit of the first 1 ms of each EPSP. Correlation analysis was performed on the timing of individual EPSPs detected

automatically in paired current clamp recordings from hilar neurons. Post stimulus correlation was assessed in a 19 s window that started 0.5 s after perforant path stimulation (average 4.3 ± 0.5 traces per paired recording). Cross correlogram time bins were 5 ms wide and were centered on zero time difference. We used exhaustive shuffle prediction (Supplementary Fig. 3b, bottom graph) to correct for expected frequency of randomly coincident EPSPs during synaptic barrages. Plots of excess correlation (Supplementary Fig. 3b,c) reflect increased frequency of near-synchronous EPSPs beyond the frequencies measured in cross correlations between shuffled episodes. All episodes compared in control and shuffled cross correlations contained similar synaptic barrages (reproducibility of responses illustrated in Fig. 8a). All data are presented as mean ± s.e.m. except where noted. Statistical significance was determined using Student's *t*-test, unless otherwise specified.

Population analysis

Cell assembly responses were based on spontaneous EPSP frequencies assessed in nonoverlapping 1 s duration windows in 2 or 3 simultaneously-recorded hilar cells. Population response trajectories in Fig. 8 illustrate EPSP frequencies in 10 windows (1 s duration) before the PP stimulation and 5 windows after stimulation. Comparisons between different responses (acquired in different episodes) were based on both Euclidean distance between up-states (average of EPSP frequencies from 0.5 to 4.5 s after the last PP stimulation; "Distance" axis in Fig. 8d) and the angle formed between mean population vectors ("Angle" axis in Fig. 8d; baseline EPSP frequency in each simultaneously-recorded hilar cell subtracted). Stimulus separability was tested by exhaustive comparisons of cross-stimuli responses (all possible stimulus A vs. stimulus B comparisons in that experiment; red symbols in Fig. 8d) and comparisons of responses evoked by the same stimulus (A or B; black and blue symbols in Fig. 8d). Statistically significance of stimulus separability employed the Hotelling T-test, a generalization of the standard T-test for multiple dimensions. Statistical significance of separability based solely on distance metrics was assessed using Student's T-test. Statistical significance of separability based solely on the angle divergence of mean population vectors was determined using the Watson-Williams two-sample test.

Population trajectory separability over time was assessed using a naive Bayes classifier generated by the mean responses recorded in 2 or 3 simultaneously-recorded hilar neurons 0.5 to 4.5 s post perforant path stimulations. This classifier was then used in two ways. First, the prior probability of each stimulus was made equal throughout the time period, generating predictions based solely on the current 1-s response window (black symbols in Fig. 8g). Second, classification of previous time epochs was fed back into the classifier to represent a downstream network that integrates prior information over time to improve its estimate. In this method priors were the average of 0.5 (to represent no previous knowledge of the stimulus) and each previous post-stimulus epoch (red symbols in Fig. 8g).

Supplementary Material

Refer to Web version on PubMed Central for supplementary material.

Acknowledgments

We thank Drs. Todd Pressler and Roberto Galan for helpful discussions during this project. We also thank Drs. Steven Jones and Jason Frazier for helpful comments on the manuscript. We thank Pavel Puzerey for technical assistance. This work was supported by National Institutes of Health (NIH) Grant R01-NS33590 to B.W.S.

References

1. Schiller J, Major G, Koester HJ, Schiller Y. NMDA spikes in basal dendrites of cortical pyramidal neurons. Nature. 2000; 404:285–289. [PubMed: 10749211]
2. Sanchez-Vives MV, McCormick DA. Cellular and network mechanisms of rhythmic recurrent activity in neocortex. Nat Neurosci. 2000; 3:1027–1034. [PubMed: 11017176]
3. Egorov AV, Hamam BN, Fransén E, Hasselmo ME, Alonso AA. Graded persistent activity in entorhinal cortex neurons. Nature. 2002; 420:173–178. [PubMed: 12432392]
4. Colombo M, Gross CG. Responses of inferior temporal cortex and hippocampal neurons during delayed matching to sample in monkeys (Macaca fascicularis). Behav Neurosci. 1994; 108:443–455. [PubMed: 7917038]
5. Fraser DD, MacVicar BA. Cholinergic-dependent plateau potential in hippocampal CA1 pyramidal neurons. J Neurosci. 1996; 16:4113–4128. [PubMed: 8753873]
6. Funahashi S, Bruce CJ, Goldman-Rakic PS. Mnemonic coding of visual space in the monkey's dorsolateral prefrontal cortex. J Neurophysiol. 1989; 61:331–349. [PubMed: 2918358]
7. Funahashi S, Chafee MV, Goldman-Rakic PS. Prefrontal neuronal activity in rhesus monkeys performing a delayed anti-saccade task. Nature. 1993; 365:753–756. [PubMed: 8413653]
8. Hampson RE, Simeral JD, Deadwyler SA. "Keeping on track": firing of hippocampal neurons during delayed-nonmatch-to-sample performance. J Neurosci. 2002; 22:RC198. [PubMed: 11784810]
9. Major G, Tank D. Persistent neural activity: prevalence and mechanisms. Curr Opin Neurobiol. 2004; 14:675–684. [PubMed: 15582368]
10. Aksay E, Gamkrelidze G, Seung HS, Baker R, Tank DW. In vivo intracellular recording and perturbation of persistent activity in a neural integrator. Nat Neurosci. 2001; 4:184–193. [PubMed: 11175880]
11. McCormick DA, Connors BW, Lighthall JW, Prince DA. Comparative electrophysiology of pyramidal and sparsely spiny stellate neurons of the neocortex. J Neurophysiol. 1985; 54:782–806. [PubMed: 2999347]
12. Spruston N, Johnston D. Perforated patch-clamp analysis of the passive membrane properties of three classes of hippocampal neurons. J Neurophysiol. 1992; 67:508–529. [PubMed: 1578242]
13. Hebb, D. The Organization of Behavior. John Wiley & Sons; New York: 1949.
14. Seung HS. How the brain keeps the eyes still. Proc Natl Acad Sci USA. 1996; 93:13339–13344. [PubMed: 8917592]
15. Abeles M, et al. Cortical activity flips among quasi-stationary states. Proc Natl Acad Sci USA. 1995; 92:8616–8620. [PubMed: 7567985]
16. Amit DJ, Mongillo G. Spike-driven synaptic dynamics generating working memory states. Neural Comput. 2003; 15:565–596. [PubMed: 12620158]
17. Goldman MS, Levine JH, Major G, Tank DW, Seung HS. Robust persistent neural activity in a model integrator with multiple hysteretic dendrites per neuron. Cereb Cortex. 2003; 13:1185–1195. [PubMed: 14576210]
18. Seung HS, Lee DD, Reis BY, Tank DW. Stability of the memory of eye position in a recurrent network of conductance-based model neurons. Neuron. 2000; 26:259–271. [PubMed: 10798409]
19. Williams PA, Larimer P, Gao Y, Strowbridge BW. Semilunar granule cells: glutamatergic neurons in the rat dentate gyrus with axon collaterals in the inner molecular layer. J Neurosci. 2007; 27:13756–13761. [PubMed: 18077687]
20. Strowbridge BW, Buckmaster PS, Schwartzkroin PA. Potentiation of spontaneous synaptic activity in rat mossy cells. Neurosci Lett. 1992; 142:205–210. [PubMed: 1454217]

21. Scharfman HE. Characteristics of spontaneous and evoked EPSPs recorded from dentate spiny hilar cells in rat hippocampal slices. J Neurophysiol. 1993; 70:742–757. [PubMed: 8105038]
22. Strowbridge BW, Schwartzkroin PA. Transient potentiation of spontaneous EPSPs in rat mossy cells induced by depolarization of a single neurone. J Physiol (Lond). 1996; 494 (Pt 2):493–510. [PubMed: 8842007]
23. Cheng S, Frank LM. New experiences enhance coordinated neural activity in the hippocampus. Neuron. 2008; 57:303–313. [PubMed: 18215626]
24. Soriano E, Frotscher M. Mossy cells of the rat fascia dentata are glutamate-immunoreactive. Hippocampus. 1994; 4:65–69. [PubMed: 7914798]
25. Scharfman HE. Electrophysiological evidence that dentate hilar mossy cells are excitatory and innervate both granule cells and interneurons. J Neurophysiol. 1995; 74:179–194. [PubMed: 7472322]
26. Buckmaster PS, Wenzel HJ, Kunkel DD, Schwartzkroin PA. Axon arbors and synaptic connections of hippocampal mossy cells in the rat in vivo. J Comp Neurol. 1996; 366:271–292. [PubMed: 8698887]
27. Larimer P, Strowbridge BW. Nonrandom local circuits in the dentate gyrus. J Neurosci. 2008; 28:12212–12223. [PubMed: 19020015]
28. Mayer ML, Westbrook GL. Permeation and block of N-methyl-D-aspartic acid receptor channels by divalent cations in mouse cultured central neurones. J Physiol (Lond). 1987; 394:501–527. [PubMed: 2451020]
29. Xu W, Lipscombe D. Neuronal Ca(V)1.3alpha(1) L-type channels activate at relatively hyperpolarized membrane potentials and are incompletely inhibited by dihydropyridines. J Neurosci. 2001; 21:5944–5951. [PubMed: 11487617]
30. Fox AP, Nowycky MC, Tsien RW. Kinetic and pharmacological properties distinguishing three types of calcium currents in chick sensory neurones. J Physiol (Lond). 1987; 394:149–172. [PubMed: 2451016]
31. Chow K, Wu C, Sui GP, Fry CH. Role of the T-type Ca2+ current on the contractile performance of guinea pig detrusor smooth muscle. Neurourol Urodyn. 2003; 22:77–82. [PubMed: 12478606]
32. Georgopoulos AP, Schwartz AB, Kettner RE. Neuronal population coding of movement direction. Science. 1986; 233:1416–1419. [PubMed: 3749885]
33. Miller LM, Recanzone GH. Populations of auditory cortical neurons can accurately encode acoustic space across stimulus intensity. Proc Natl Acad Sci USA. 2009; 106:5931–5935. [PubMed: 19321750]
34. MacLean JN, Watson BO, Aaron GB, Yuste R. Internal dynamics determine the cortical response to thalamic stimulation. Neuron. 2005; 48:811–823. [PubMed: 16337918]
35. Acsády L, Kamondi A, Sík A, Freund T, Buzsáki G. GABAergic cells are the major postsynaptic targets of mossy fibers in the rat hippocampus. J Neurosci. 1998; 18:3386–3403. [PubMed: 9547246]
36. Scharfman HE. Dentate hilar cells with dendrites in the molecular layer have lower thresholds for synaptic activation by perforant path than granule cells. J Neurosci. 1991; 11:1660–1673. [PubMed: 2045880]
37. Ishizuka N, Weber J, Amaral DG. Organization of intrahippocampal projections originating from CA3 pyramidal cells in the rat. J Comp Neurol. 1990; 295:580–623. [PubMed: 2358523]
38. Scharfman HE. Evidence from simultaneous intracellular recordings in rat hippocampal slices that area CA3 pyramidal cells innervate dentate hilar mossy cells. J Neurophysiol. 1994; 72:2167–2180. [PubMed: 7884451]
39. Jefferys JG. Nonsynaptic modulation of neuronal activity in the brain: electric currents and extracellular ions. Physiol Rev. 1995; 75:689–723. [PubMed: 7480159]
40. Williams SR, Tóth TI, Turner JP, Hughes SW, Crunelli V. The ‘window’ component of the low threshold Ca2+ current produces input signal amplification and bistability in cat and rat thalamocortical neurones. J Physiol (Lond). 1997; 505 (Pt 3):689–705. [PubMed: 9457646]
41. Wei DS, et al. Compartmentalized and binary behavior of terminal dendrites in hippocampal pyramidal neurons. Science. 2001; 293:2272–2275. [PubMed: 11567143]

42. Hughes SW, Cope DW, Tóth TI, Williams SR, Crunelli V. All thalamocortical neurones possess a T-type Ca2+ 'window' current that enables the expression of bistability-mediated activities. J Physiol (Lond). 1999; 517 (Pt 3):805–815. [PubMed: 10358120]

43. Lo F, Erzurumlu RS. L-type calcium channel-mediated plateau potentials in barrelette cells during structural plasticity. J Neurophysiol. 2002; 88:794–801. [PubMed: 12163531]

44. Koschak A, et al. Molecular nature of anomalous L-type calcium channels in mouse cerebellar granule cells. J Neurosci. 2007; 27:3855–3863. [PubMed: 17409250]

45. Talley EM, et al. Differential distribution of three members of a gene family encoding low voltage-activated (T-type) calcium channels. J Neurosci. 1999; 19:1895–1911. [PubMed: 10066243]

46. Marr D. Simple memory: a theory for archicortex. Philos Trans R Soc Lond, B, Biol Sci. 1971; 262:23–81. [PubMed: 4399412]

47. Sass KJ, et al. Specificity in the correlation of verbal memory and hippocampal neuron loss: dissociation of memory, language, and verbal intellectual ability. J Clin Exp Neuropsychol. 1992; 14:662–672. [PubMed: 1474137]

48. Smith DH, Lowenstein DH, Gennarelli TA, McIntosh TK. Persistent memory dysfunction is associated with bilateral hippocampal damage following experimental brain injury. Neurosci Lett. 1994; 168:151–154. [PubMed: 8028769]

49. Lothman EW, Stringer JL, Bertram EH. The dentate gyrus as a control point for seizures in the hippocampus and beyond. Epilepsy Res Suppl. 1992; 7:301–313. [PubMed: 1334669]

50. Halasy K, Somogyi P. Subdivisions in the multiple GABAergic innervation of granule cells in the dentate gyrus of the rat hippocampus. Eur J Neurosci. 1993; 5:411–429. [PubMed: 8261118]

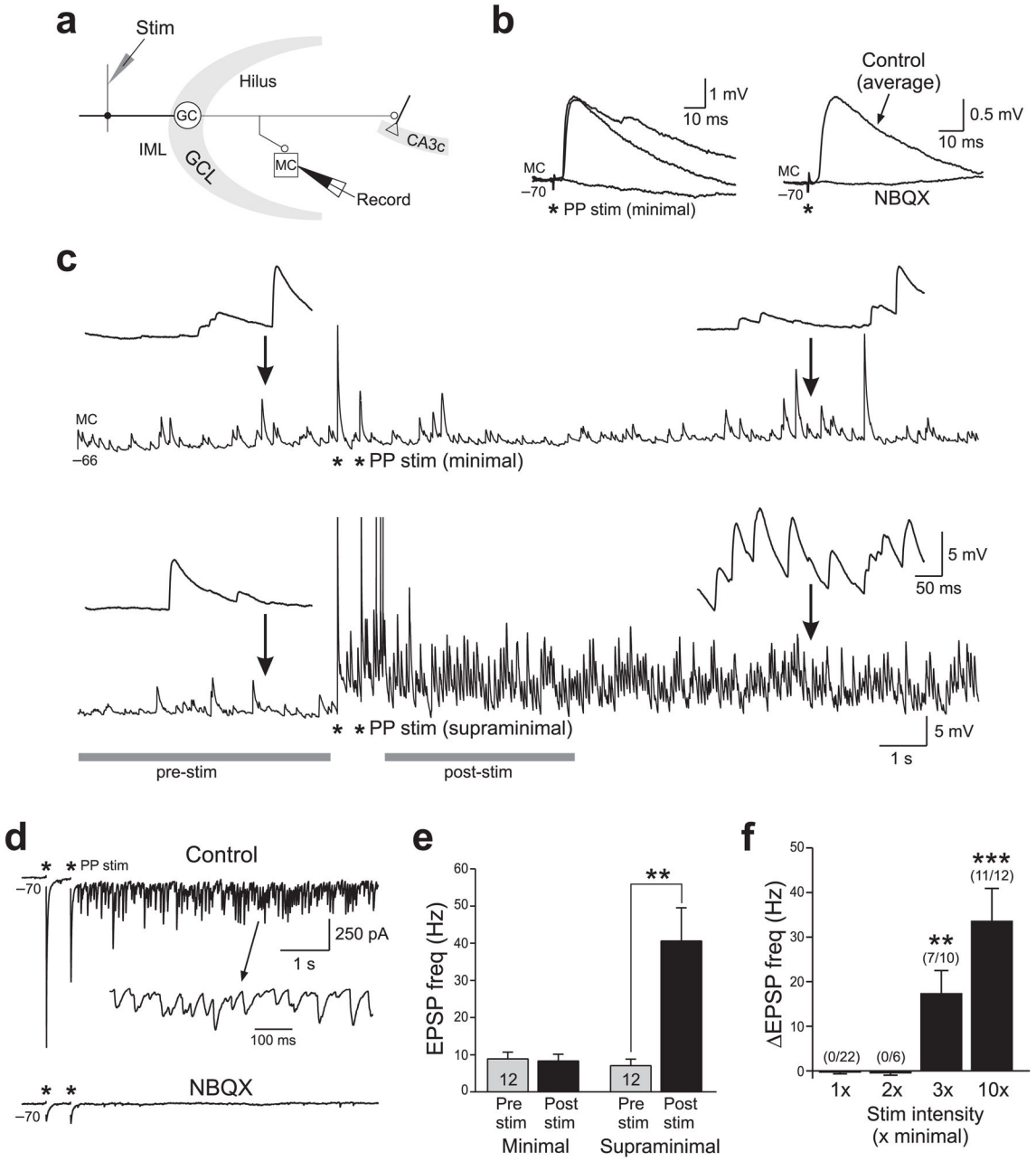

Figure 1. Long-lasting synaptic barrages in hilar neurons evoked by perforant path stimulation

(**a**) Schematic diagram illustrating stimulating electrode in the PP (*Stim*) and an intracellular recording of a mossy cell (*Record*). (**b**) Minimal stimulation (*asterisks*) evoked disynaptic EPSPs and failures in a hilar neuron (left). Mean response blocked by NBQX (10 μM; right). Baseline membrane potential indicated below trace. (**c**) Minimal PP stimulation had no effect on the frequency of spontaneous EPSPs recorded in a mossy cell. Supraminimal PP stimulation (*bottom*) triggered a long-lasting increase in spontaneous EPSP frequency. *Insets* illustrate expanded examples of voltage recordings before and after PP stimulation. *Grey bars* indicate time epochs used for EPSP frequency analysis. (**d**) PP-evoked EPSC barrage

blocked by 5 μM NBQX in a voltage-clamped hilar cell. *Inset* shows expanded record of PP-evoked EPSC barrage. (**e**) Comparison of EPSP frequency before and after PP stimulation in hilar cells. ** P <0.001. Number of cells indicated at bottom of bars. (**f**) Plot of increase in EPSP frequency following PP stimulation in response to 1x, 2x, 3x and 10x minimal stimulus intensity. ** P<0.01, *** P<0.001. Error bars represent s.e.m. Fraction of hilar cells tested in which EPSP frequency increased at least 2-fold over basal frequencies indicated in parenthesis above each bar. Minimal PP stimulus intensity was 22.5±1.6 μA in these experiments.

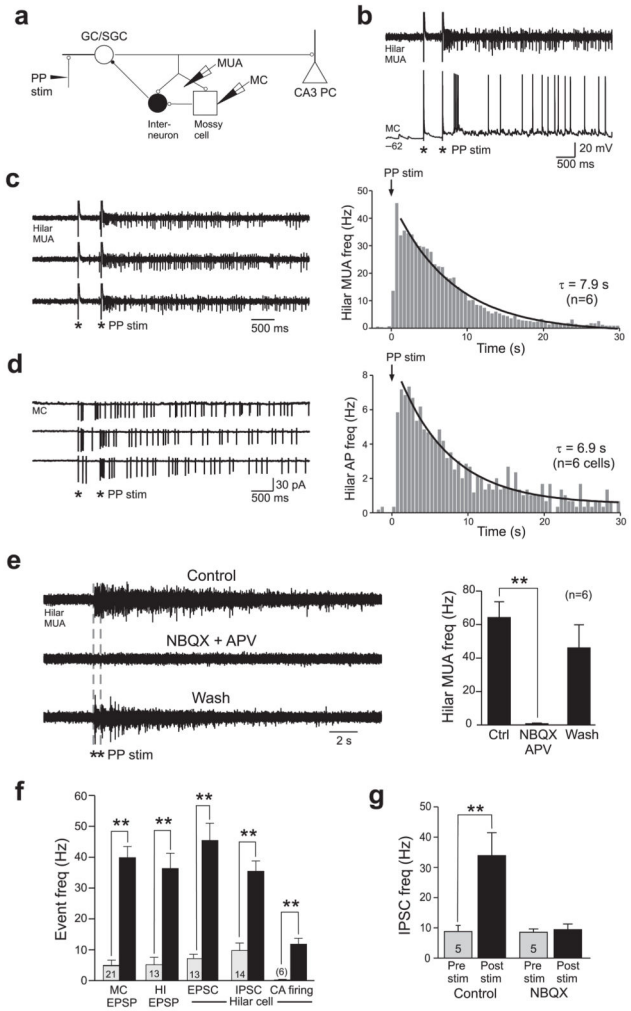

Figure 2. Hilar up-states require glutamatergic synaptic inputs

(**a**) Schematic diagram showing extracellular multiunit recording electrode (MUA) and patch-clamp recording electrode in hilus. (**b**) Supraminimal PP stimulation (*asterisks*) triggers prolonged spiking in an intracellularly-recorded hilar mossy cell (*bottom*) and in nearby hilar neurons (*top*, simultaneous MUA record). (**c**) Repeated PP stimuli evoked long-duration hilar MUA discharges. *Right*, time course of hilar neuron spiking quantified in 6 MUA experiments. (**d**) Cell-attached responses from a mossy cell to repeated PP stimulation. *Right*, time course of cell-attached hilar cell activity in 6 cells. (**e**) PP-evoked hilar up-states recorded extracellular are reversibly abolished by blockade of ionotropic glutamate receptors with NBQX (5 μM) and D-APV (25 μM). *Right*, summary of effects of NBQX and APV on hilar up-states in 6 MUA experiments. ** $P<10^{-4}$. (**f**) Changes in synaptic event frequency before and 0.5–4.5 s after PP stimulation. Up-states with increased frequency of EPSPs recorded in physiologically-identified mossy cells (*MC*) and hilar interneurons (*HI*). Up-states also associated with increased frequency of excitatory (*EPSC*) and inhibitory (*IPSC*) synaptic inputs recorded in voltage-clamped hilar cells (at −80 and +15 mV, respectively). Up-states also associated with increased frequency hilar cell firing in cell-attached recordings (*CA Firing*). ** $P<10^{-4}$ for each comparison. (**g**) Increases in

inhibitory barrages during PP-evoked hilar up-states are abolished by 5 μM NBQX. ** $P<0.01$.

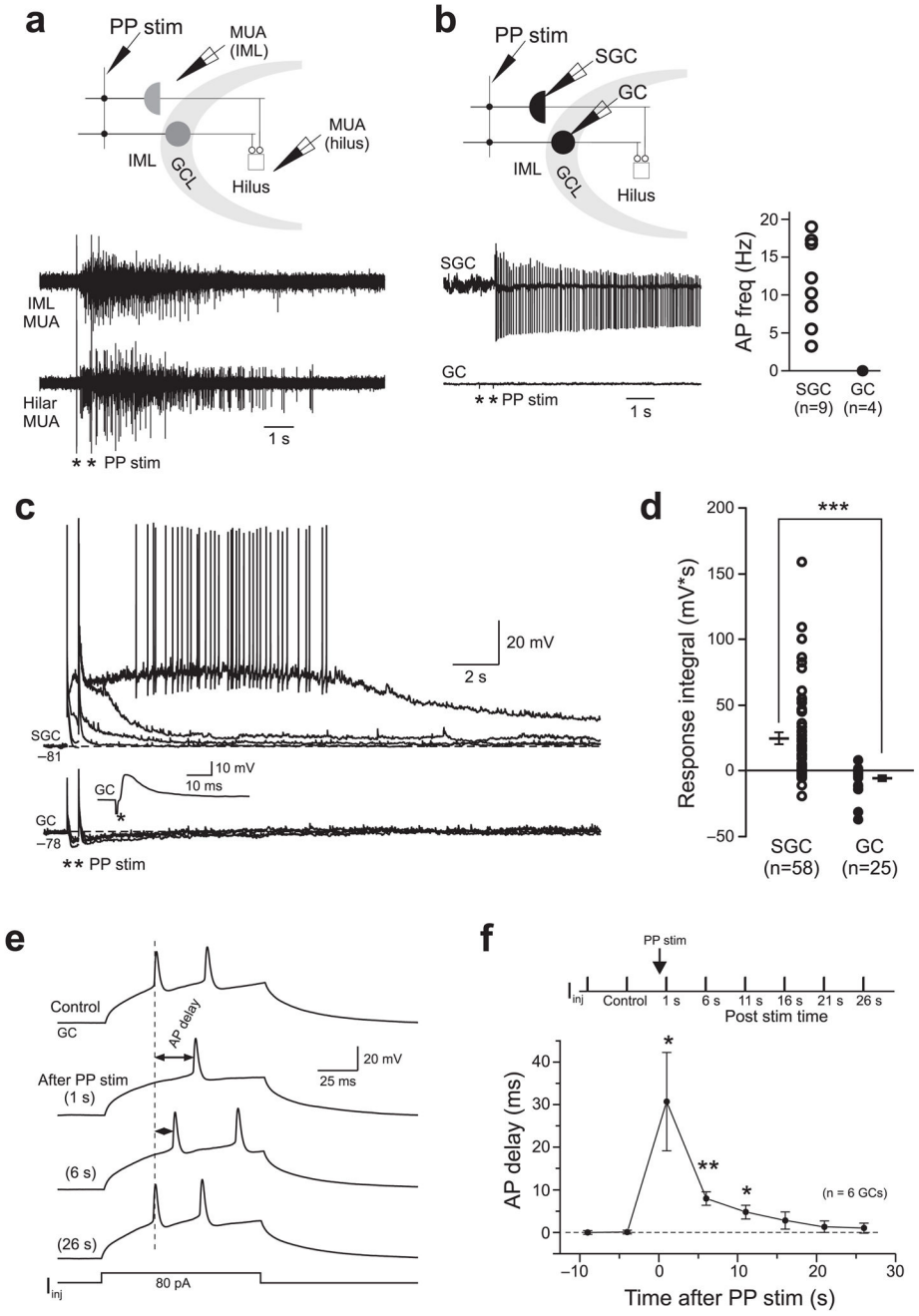

Figure 3. PP stimulation evokes plateau potentials and persistent firing in SGCs

(**a**) Persistent firing recorded simultaneously in hilar and IML MUA electrodes in response to PP stimulation. Schematic of simultaneous MUA recording in hilus and inner molecular layer (*IML*) shown above recordings. (**b**) *Left*, cell-attached recordings of responses to PP stimuli in SGC (open symbols) and GCs (closed symbols). *Right*, PP stimulation evoked persistent firing in 9/9 SGCs (mean frequency = 11.6±2.2 Hz; significantly greater than 0 Hz; $P<0.001$; one sample t-test) and 0/4 GCs tested. Diagram illustrating recording configuration shown above plots. (**c**) Intracellular responses to graded PP stimulation in an SGC (*top*) and GC (*bottom*, not simultaneous with SGC). Monosynaptic GC EPSP shown in

inset. (**d**) Plot of responses to PP stimuli (integral from 0.5–4.5 s after last PP stimulus, recorded at ~−70 mV) in 58 SGCs and 25 GCs. Mean stimulus intensities within 3 μA (and not statistically different, $P>0.05$), and mean membrane potentials within 3 mV, between populations of SGCs and GCs compared. *** $P<10^{-4.}$. **(e)** Prolonged functional inhibition of granule cells following PP stimulation. Example responses to identical depolarizing steps before (*Control*) and 1, 6 and 26 s after PP stimulation. **(f)** Plot of functional inhibition of GCs following PP stimulation. Inhibition assessed by increased latency to first action potential in responses to depolarizing steps. Diagram above plot indicates timing of 8 current pulses used to assess inhibition (2 control and 6 after PP stimulation). * $P<0.05$, ** $P<0.005$ (2-tailed *t*-test; $n=6$ GCs)

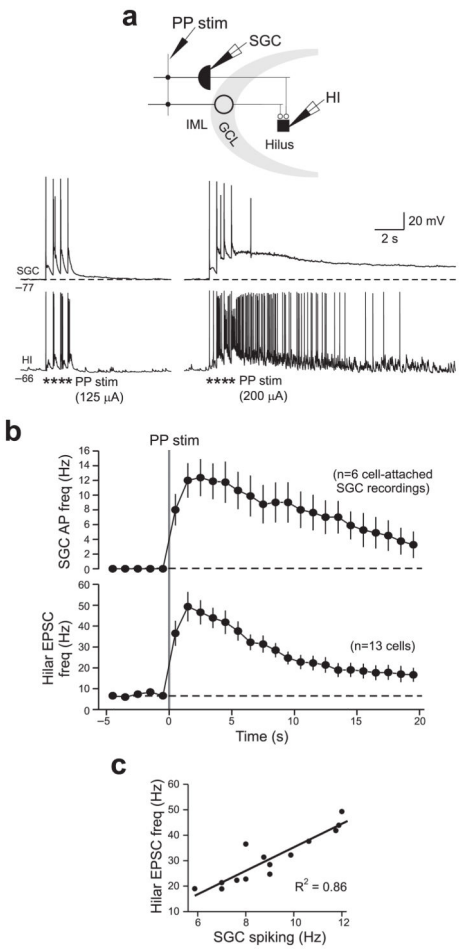

Figure 4. Correlation between plateau potentials in SGCs and hilar up-states following PP stimulation

(**a**) Responses of SGC and hilar interneuron (*HI*) to graded PP stimulation. Lower intensity PP stimulation (125 μA) failed to evoke plateau potentials in the SGC and synaptic barrages in the HI. Increasing stimulation intensity to 200 μA triggered both plateau potentials and hilar synaptic barrages (recorded simultaneously). Schematic diagram illustrating simultaneous intracellular recordings of SGCs and hilar neurons shown above records. (**b**) Plots of change in persistent firing frequency in 6 cell-attached SGC recordings (*top*) and EPSC frequency following PP stimulation in 13 voltage-clamp hilar cell recordings. Mean EPSP frequency±s.e.m. calculated over 1 s response windows. SGC discharge frequency and hilar cell synaptic responses significantly correlated. (**c**) Plot of correlation (R^2=0.86, measured between 0 and 15 s after last PP stimulus) between hilar EPSC frequency and SGC firing measured in cell-attached recordings.

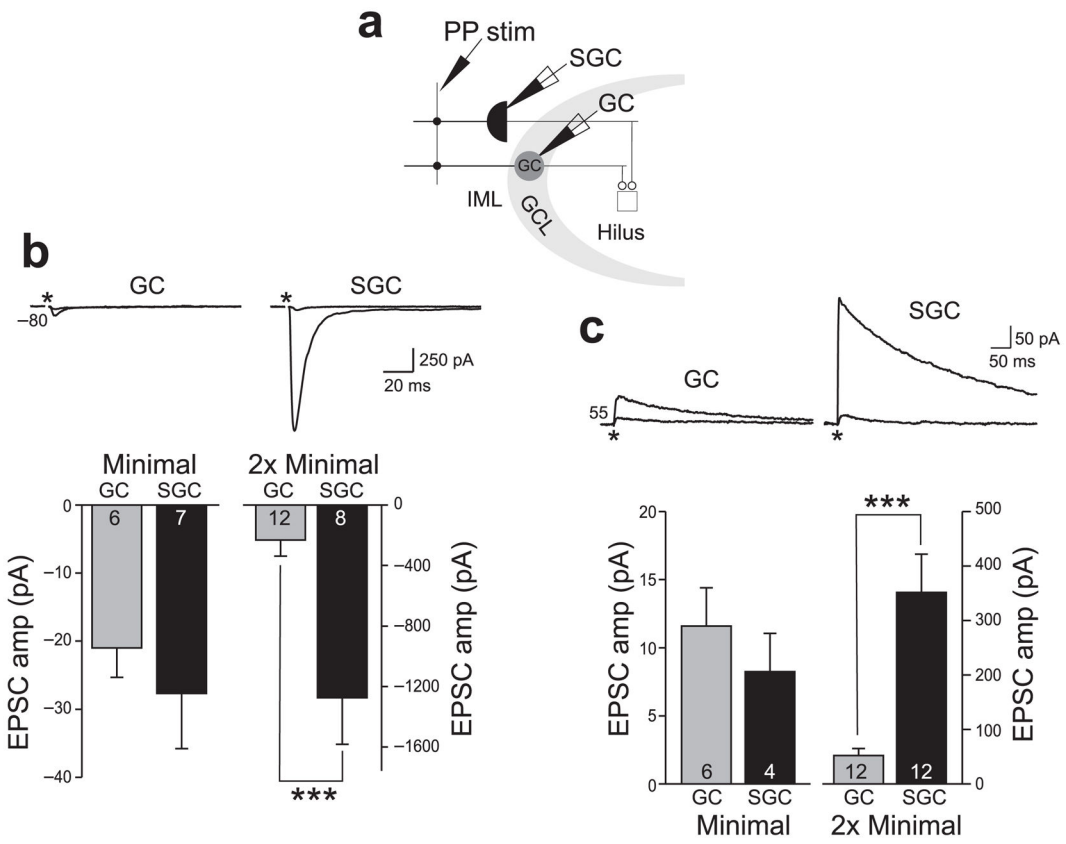

Figure 5. SGCs receive large-amplitude glutamatergic inputs

(**a**) Schematic diagram of SGC and GC recording configurations (not simultaneous). (**b**) Comparison of voltage-clamp responses recorded at −80 mV to minimal and 2x minimal PP stimulation in GCs and SGCs. Peak EPSC amplitude was not statistically different between GCs and SGCs at minimal intensities ($P>0.05$) but differed by more than 5-fold at 2x minimal intensity. *** $P<0.001$. Superimposed example minimal and 2x minimal GC and SGC responses shown above bar graphs. (**c**) Parallel analysis for NMDA receptor-mediated EPSC response in GCs and SGCs (responses recorded at +55 mV, response amplitude measured 100 ms after stimulation). Minimal NMDA receptor responses were not different ($P>0.05$) while responses to 2 x minimal stimulation differed by more than 6-fold between GCs and SGCs. *** $P<0.005$. Increasing stimulus intensity from 1x to 2 x minimal levels increased NMDA receptor EPSC amplitude by 5-fold in GCs and 43-fold in SGCs.

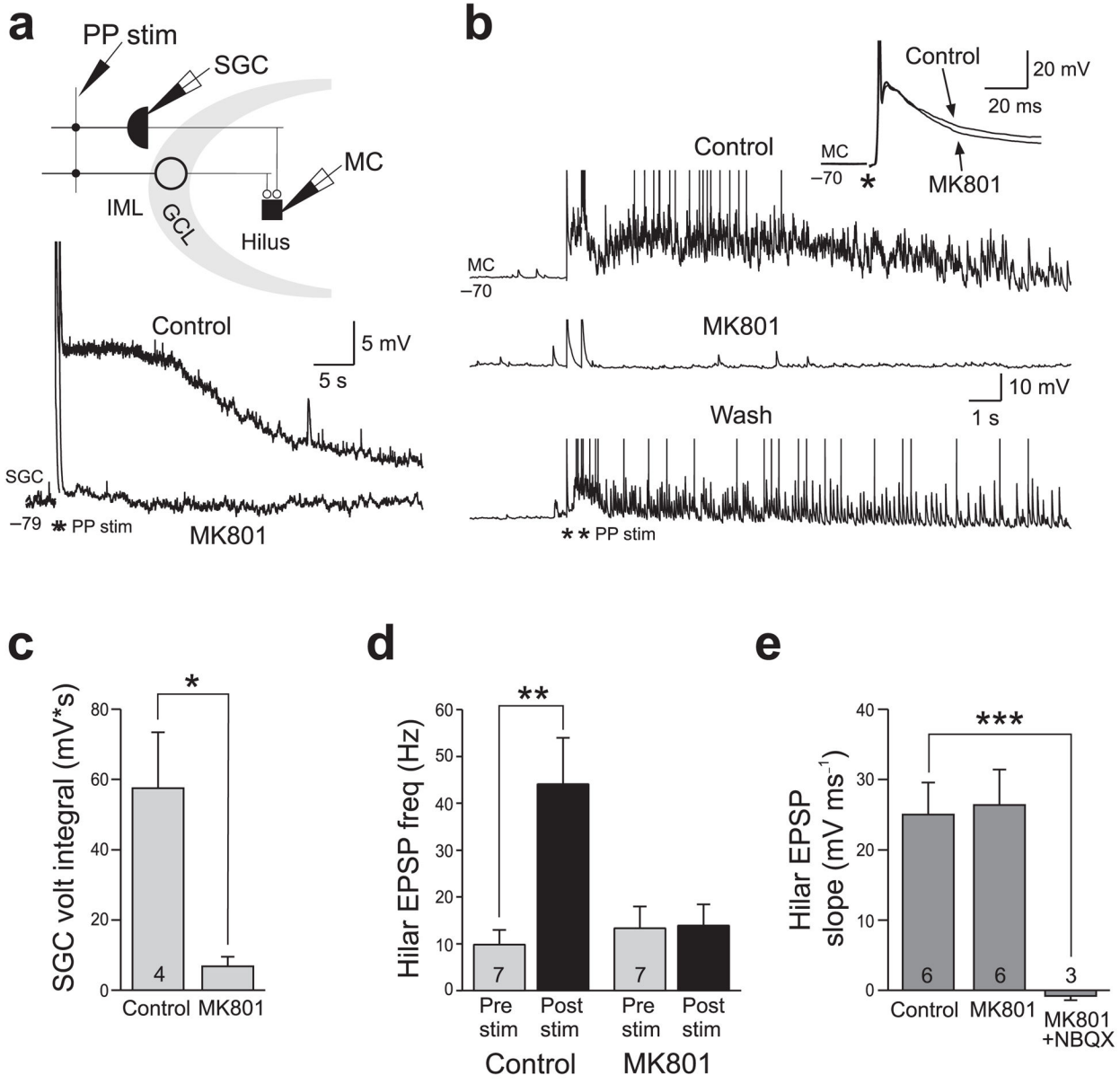

Figure 6. Plateau potentials in SGCs activated by NMDA receptors

(**a**) SGC responses to PP stimulation before and after bath application of MK801 (10 μM). Schematic diagram of SGC and hilar cell recording configurations (not simultaneous) shown above records. (**b**) MK801 reversibly blocked synaptic barrages evoked by PP stimulation recorded in hilar neurons without affecting disynaptic evoked EPSPs (*inset*). (**c**) Plot of mean PP-evoked plateau response integrals before (*Control*) and after 10 μM MK801 in 4 SGCs. * $P<0.02$. (**d**) Plot of mean PP-evoked change in EPSP frequency before and after MK801 in 7 hilar neurons. ** $P<0.005$. Pre-stimulus EPSP frequency was not significantly increased by MK801 (9.8 Hz before vs. 13.3 Hz after MK801; $P>0.05$). (**e**) Plot of disynaptic EPSP slope before and after MK801 in 6 hilar neurons ($P>0.05$). The

combination of NBQX and MK801 abolished evoked EPSPs in 3 hilar cells tested. *** $P<0.005$.

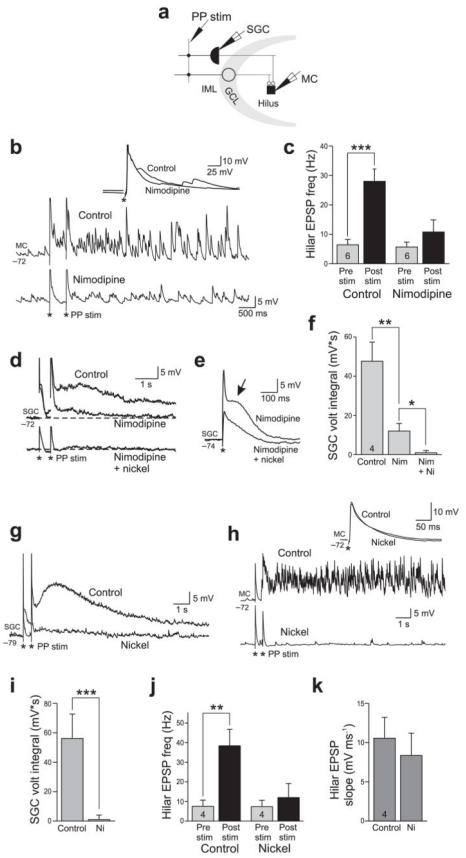

Figure 7. Both plateau potentials in SGCs and synaptic barrages in hilar neurons require L- and T-type VGCCs

(**a**) Schematic diagram illustrating recording configurations (not simultaneous). (**b**) PP-evoked synaptic barrages in a hilar cell was attenuated by 10 μM nimodipine. *Inset* shows short-latency EPSP that was unaffected by nimodipine. (**c**) Summary of the effect of 10 μM nimodipine on EPSP frequency during synaptic barrages in 6 hilar neurons. *** $P<0.005$. (**d**) Nimodipine also blocked most of the plateau response in an SGC (20 μM). Subsequent addition of 200 μM Ni abolished the nimodipine-resistant plateau response. (**e**) Enlargement of initial response in nimodipine and in nimodipine + Ni. *Arrow* indicates short-duration plateau response blocked by Ni. (**f**) Summary of the effects of nimodipine (*Nim*) and nimodipine plus Ni (*Nim + Ni*) on plateau responses in 4 SGCs. ** $P<0.02$; * $P<0.05$. (**g**) SGC responses to PP stimulation before and after application of nickel (200 μM). *Inset* shows monosynaptic EPSP evoked by first PP stimulus was unaffected by nickel. (**h**) Nickel (200 μM) also blocked synaptic barrages evoked by PP stimulation recorded in hilar cells. *Inset* shows disynaptic mossy cell EPSP was unaffected by nickel. (**i**) Plot of mean PP-evoked plateau response integrals before (*Control*) and after 200 μM nickel (*Ni*) in 6 SGC recordings. *** $P<0.005$. (**j**) Plot of mean PP-evoked change in EPSP frequency before and after nickel in 4 hilar cell recordings. ** $P<0.005$. (**k**) Plot of disynaptic EPSP slope before and after nickel in 4 hilar neurons ($P>0.05$).

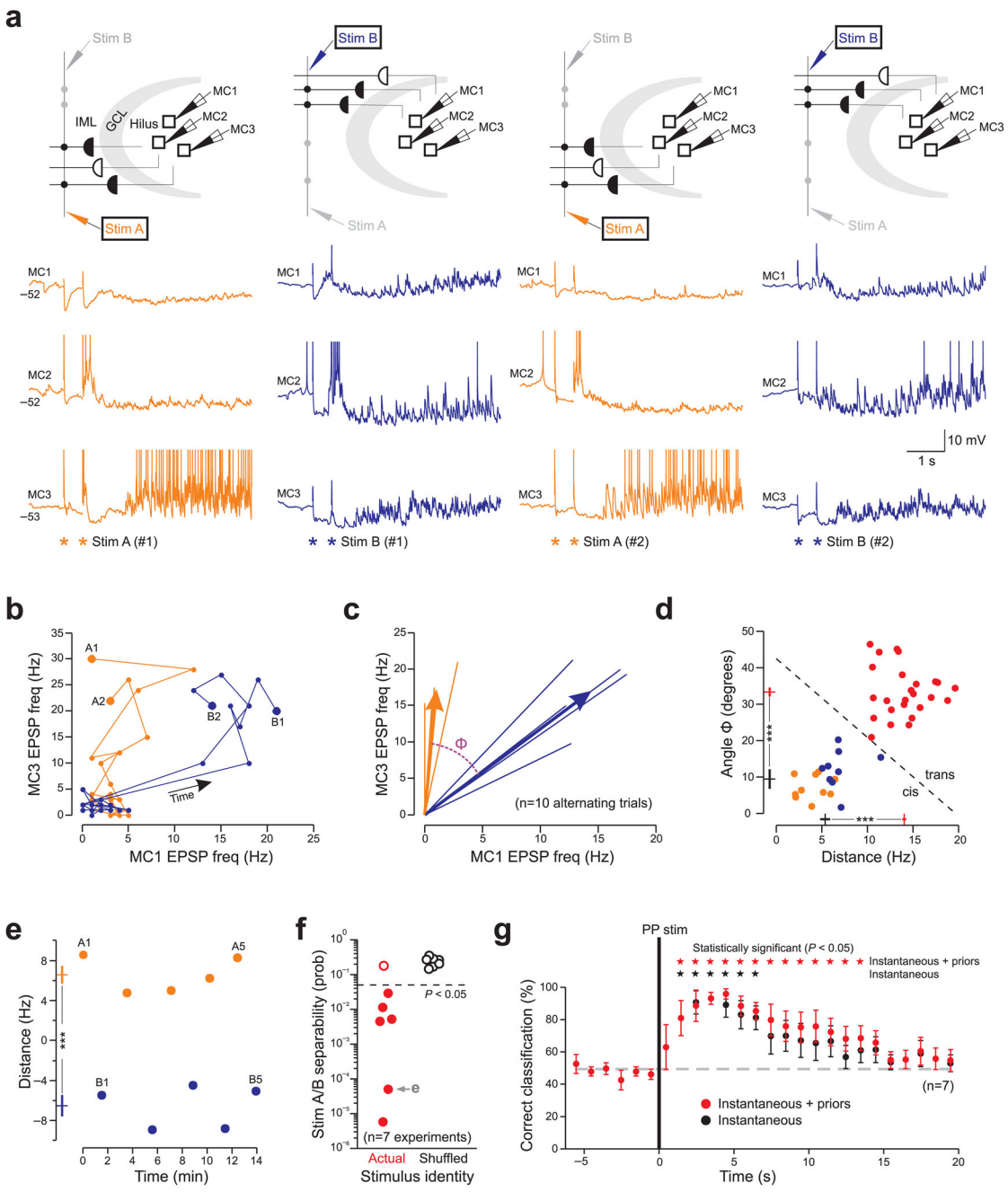

Figure 8. PP-evoked up-states generate hilar cell assemblies that encode stimulus identity

(**a**) Responses to two different stimulation electrodes (*A*, *orange* traces and *B*, *blue* traces) recorded simultaneously in three mossy cells (*MCs*). Responses from two consecutive, alternating *A/B* sequences). (**b**) Plot of EPSP frequency for the four episodes shown in **a**. EPSP frequency calculated in 1 s response windows. (**c**) Average trajectory vectors for 10 alternating *A/B* responses in the same simultaneous triple recording shown in **a**. Vectors generated from individual episodes indicated by thin lines. Difference between mean population responses to stimulus *A* and *B* quantified by Euclidean distance and angle (√) between mean response vectors. (**d**) Plot of difference in angle (√) vs. distance between

vector representations of network responses to stimuli *A* and *B* (*red* symbols). Comparisons between different stimuli (*A* and *B*) denoted "*trans*" in plot. Comparisons between responses to the same stimulus site denoted "*cis*". Dashed line indicates separation plane between *cis* and *trans* response differences estimated using linear discriminant analysis. Mean vector angle and distance metrics for *cis* and *trans* differences indicated inside X (distance) and Y (angle) axes. *** $P<10^{-6}$. (**e**) Plot of distance from an optimal *A/B* response classification plane constructed in EPSP frequency space for 10 consecutive responses in the same triple mossy cell recording shown in **a**. Mean responses to stimuli *A* and *B* indicated inside Y axis. *** $P<10^{-5}$. (**f**) Plot of statistical significance for *A/B* response comparisons in 7 experiments similar to **e**. Population responses to stimuli A and B were statistically distinguishable in 6 of 7 experiments (*filled red symbols*; "*Actual*"; example shown in **e** indicated by *grey arrow*). Comparisons of the same responses with stimulus identity shuffled yielded no statistically significant differences (*black symbols*). *Open symbols* indicate $P>0.05$. (**g**) Plot of predictions of stimulus identity based on 1 s duration response windows in 7 simultaneous 2- and 3-hilar cell recordings. *Black symbols* indicate prediction accuracy (mean±s.e.m.) from moving 1 s windows; *black asterisks* indicate windows that predicted stimulus identity more accurately than chance over 7 experiments ($P<0.05$). *Red symbols* indicate prediction accuracy from nonoverlapping 1 s duration windows including predictions from prior windows. *Red asterisks* indicate cumulative prediction accuracies significantly above chance ($P<0.05$).